


Superconductivity and equation of state of lanthanum at megabar pressuresWuhao Chen,¹ Dmitrii V. Semenov,² Ivan A. Troyan,³ Anna G. Ivanova,³ Xiaoli Huang,^{1,*}
Artem R. Oganov,² and Tian Cui^{4,1,†}¹State Key Laboratory of Superhard Materials, College of Physics, Jilin University, Changchun 130012, China²Skolkovo Institute of Science and Technology, Skolkovo Innovation Center, 3 Nobel Street, Moscow 143026, Russia³Shubnikov Institute of Crystallography, Federal Scientific Research Center Crystallography and Photonics, Russian Academy of Sciences, Moscow 119333, 59 Leninskii Prospekt, Russia⁴School of Physical Science and Technology, Ningbo University, Ningbo 315211, China (Received 6 March 2019; revised 13 June 2020; accepted 24 August 2020; published 26 October 2020)

Lanthanum (La) is the first member of the lanthanoid that has recently raised considerable interest because of its unique La superhydride LaH₁₀ and its own superconducting properties. There has been a lack of experimental evidence for the equation of state (EOS) and superconductivity of La at pressures exceeding one megabar. Here, we extend the pressure range up to 140 GPa to explore the EOS and superconductivity of La via the electrical resistance and x-ray diffraction measurements. We identified the phase transition sequences by the La Bail refinements of the experimental XRD patterns and discovered a distorted fcc-La phase (space group *Fmmm*) above 78 GPa with nonhydrostatic pressure transmitting media. All the experimental pressure-volume data were fitted by the third-order Birch-Murnaghan equation: $V_0 = 37.5 \text{ \AA}^3$, $B_0 = 14.5 (1) \text{ GPa}$, and $B'_0 = 5$. Superconductivity still existed in the distorted fcc-La with an onset critical temperature T_c of 9.6 K at 78 GPa, which decreases to 2.2 K at 140 GPa. We calculated the superconducting parameters of La at several pressure points, and discussed the difference from experimental T_c .

DOI: [10.1103/PhysRevB.102.134510](https://doi.org/10.1103/PhysRevB.102.134510)**I. INTRODUCTION**

Since the discovery of superconductivity (SC) in 1911 [1], scientists have searched for materials that can conduct electricity without resistance below the superconducting transition temperature (T_c). So far, tremendous efforts have been devoted to explore the high- T_c SC in a variety of materials such as cuprates [2], ion-based superconductors [3], and hydrogen-rich compounds [4]. Among them, the SC in hydrides has been successfully realized with the discovery of novel compounds in the H-S system at high pressures with the T_c of up to 203 K. The discovery of high-temperature superconductivity in *Im* $\bar{3}m$ -H₃S by theoretical [5,6] and experimental [7–9] methods hints that even a room-temperature SC can be achieved in hydrogen-rich materials. Hence, the search for superconducting polyhydrides at very high pressures has brought about a new round of research upsurge in physics of superconductors. Metal hydrides are interesting materials for realizing high- T_c superconductivity when they form unusually high stoichiometric ratios. In particular, metal lanthanum (La) can react with hydrogen yielding *Fm* $\bar{3}m$ -LaH₁₀, which has recently been reported as a high- T_c superconductor with the critical temperature above 250 K at 170 GPa [10,11]. In the framework of the total experimental and theoretical investigation of the La-H system, a study of structural and electronic properties of metal La at ultrahigh pressures is necessary

for better understanding the roles of La and H atoms in the observed SC.

The unique physical and chemical properties of rare-earth metals have attracted interest for decades. The mostly trivalent rare-earth metals from La through Lu possess a similar *d*-electron character near Fermi energy, none of them superconducting at ambient pressure except metal La [12]. As the first member of the lanthanoid, La can exist in both double hexagonal-close-packed (dhcp) phase and face-centered cubic (fcc) phase, while a bcc structure is favorable at high temperatures near the melting point [13–15]. Due to a high electronic density of states at Fermi surface and a specific phonon spectrum, one would expect a strong electron-phonon coupling, and, therefore, a reasonably high superconducting transition temperature for La. The dhcp and fcc phases yield the superconducting transition temperatures T_c near 5 and 6 K at ambient pressure, respectively [16,17]. Both structures show significant increase in T_c with pressure ($dT_c/dP \sim 0.87\text{--}1 \text{ K/GPa}$) [18,19]. The dhcp phase undergoes several structural transformations, first transforming to the fcc structure near 2.2 GPa, then to a distorted fcc (*R* $\bar{3}m$) structure at about 5.4 GPa, then returning to the original fcc phase at 60 GPa [16–18]. At the same time, the critical temperature demonstrates a complex behavior with several “waves” (broad maxima) and anomalies up to 50 GPa [18]. Inconsistent with this dfcc-fcc transition, two subsequent studies revealed that *hR*24-La (or closely related phase) phase can be preserved up to 180 GPa under quasihydrostatic pressures [10,20].

In contrast to the previous reports, we compressed the lanthanum sample in the solid-state pressure mediums (MgO

*Corresponding author: huangxiaoli@jlu.edu.cn†Corresponding author: cuitian@jlu.edu.cn

and Al_2O_3) up to 140 GPa. A new distorted fcc-La phase was discovered with $Fm\bar{m}m$ symmetry above 78 GPa. Superconductivity survives in La with critical temperature T_c of 2.2 K at 140 GPa. We have also extrapolated the upper critical magnetic field $\sim 0.32\text{--}0.43$ T upon the applied magnetic field at 140 GPa.

II. EXPERIMENTAL AND THEORETICAL METHODS

We used the target La sample purchased from Alfa Aesar with the purity of 99.9% and performed *in situ* high-pressure XRD patterns in two experimental runs. In run 1, the x-ray diffraction (XRD) measurements are conducted on synchrotron beamline 16-BMD at Advanced Photon Source using a focused monochromatic x-ray beam ($\lambda = 0.434 \text{ \AA}$) in the pressure range of 7–140 GPa. In run 2, the XRD patterns of the La sample in a pneumatic DAC with a 50- μm culet were recorded on the ID27 synchrotron beamline at the European Synchrotron Radiation Facility (Grenoble, France) with $\lambda = 0.3738 \text{ \AA}$ in the pressure range of 104–133 GPa. In both experimental runs, MgO was used as a pressure transmitting medium (PTM) and pressure gauge [21]. The CeO_2 standard was used for the calibration of the experimental parameters (sample-to-detector distance, detector's tilt angle, and the beam center). The experimental XRD images were analyzed and integrated using the DIOPAS software package (version 0.4) [22].

For electrical resistance measurements, we have used a piston-cylinder diamond anvil cell (DAC) made of a Be-Cu material, and the diamonds had a culet of 100 μm in diameter beveled at 8° to a diameter of about 300 μm . The sample chamber consisted of a tungsten gasket with a Al_2O_3 insulating layer. The excess Al_2O_3 was also used as the PTM. The piston diamond was coated with four 1- μm -thick Mo electrodes connected to the external wires using a combination of 5- μm -thick Pt shoes soldered onto brass holders. The pressure was determined from the Raman shift of the diamond-anvil edge excited with a 532-nm laser [23].

The calculations of the superconducting transition temperature T_c were carried out using the QUANTUM ESPRESSO (QE) package [24]. The phonon frequencies and electron-phonon coupling (EPC) coefficients were computed using density-functional perturbation theory [25], employing the plane-wave pseudopotential (PP) method and the Perdew-Burke-Ernzerhof and Perdew-Zunger exchange-correlation functionals [26]. In our *ab initio* calculations of the electron-phonon coupling (EPC) parameter λ , the first Brillouin zone was sampled using $2 \times 2 \times 2$ and $4 \times 4 \times 4$ q -point meshes, and a denser $24 \times 24 \times 24$ k -point mesh (with Gaussian smearing and $\sigma = 0.025$ Ry, which approximates the zero-width limit in the calculation of λ). The critical temperature T_c was calculated using the Allen-Dynes formula [27].

III. RESULTS AND DISCUSSION

The EOS of the metallic La has been investigated in the DAC and MgO was used as the PTM for two experimental runs. The synchrotron XRD patterns at various pressures are shown in Fig. S1 of the Supplemental Material [28]. The

selected Rietveld refinements of experimental XRD are presented in Fig. 1(a) and the refined lattice parameters and volume of this distorted fcc-La structure at various pressures can be seen in Table S1 of the Supplemental Material [28]. In run 1, during the compression from 17 to 49 GPa, the relative intensity of superstructure reflection (101) of *d*-fcc La between 9° and 10° decreases gradually (Fig. S1), consistent with the previously reported hcp to fcc phase transition [17]. Meanwhile, we observed that diffraction peaks (006) and (202) have different rate of shift with pressure which broadens the main peak. With further compression, diffraction peaks (200) and (220) of fcc-La start to broaden at about 78 GPa that means the beginning of distortion. Comparing with other two possible phases ($Fm\bar{3}m$ and $R\bar{3}m$) at 123 GPa (Fig. S2 [28]), we found that the distorted fcc-La structure (with space group $Fm\bar{m}m$) could fit the experimental patterns best.

Under ultrahigh pressure we shouldn't ignore that the nonhydrostatic condition can also cause this phenomenon because of macroscopic stress including gradient stress, uniaxial stress, and microscopic stress [29]. There is some evidence to help us analyze the possibilities. First, the La sample is quite small and the detection area of x-ray beam is limited to a few-micron range where the pressure is almost uniform [30]. This helps to reduce the influence of stress gradient. Second, although the uniaxial stress can lead to the same distortion, especially when the sample bridges the diamond, this would produce preferred orientation which we didn't observe. Third, considering that our metal sample is softer than Al_2O_3 and MgO at ambient pressure, the sample itself can also work as a PTM no matter how hard the pressure medium is. Importantly, from the pressure dependence of XRD, we can see that not all the peaks become broadened upon compression; especially the full width at half maximum (FWHM) of the strongest peak [indexed as a (111) peak in the $Fm\bar{3}m$ phase] keeps nearly constant from 56 GPa to the highest pressure without broadening (Fig. S1 [28]). This means that the distortion of fcc structure really happened mainly not because of the gradient or microscopic stress distribution on the sample, but is likely derived from the structural change.

Moreover, we have checked the relative enthalpy at 60–140 GPa (Fig. S3 [28]), and found that the enthalpy difference between the $Fm\bar{3}m$ and $Fm\bar{m}m$ structures is just a few meV/atom or lower which is close to the accuracy limit of DFT methods. By taking into account the Gibbs free energy at 300 K, the $Fm\bar{m}m$ -La phase is more stable than the $Fm\bar{3}m$ phase at pressures over 135 GPa. Two recent studies claimed that hcp-La can be preserved up to at least 170 GPa, even without transition to fcc structure when better PTM (H_2 , Ne, or *AB*) were used [10,20]. Their XRD patterns reveal the super-structure reflections which were used to distinguish the fcc from hcp phase in Ref. [17]. We also observed this in our run 2 and the peaks were marked with asterisks in Fig. 1(b), however, the effects of impurities such as lanthanum monoxide (LaO) can't be ruled out [31,32]. Since we reproduced the reported hcp to fcc phase transition in run 1, the distortion of fcc-La with MgO as the PTM is credible.

The plots of EOSs show the anisotropic behavior of the $Fm\bar{m}m$ La sample under pressure: da/dP and db/dP are close and can be roughly approximated by linear functions $a(P) =$

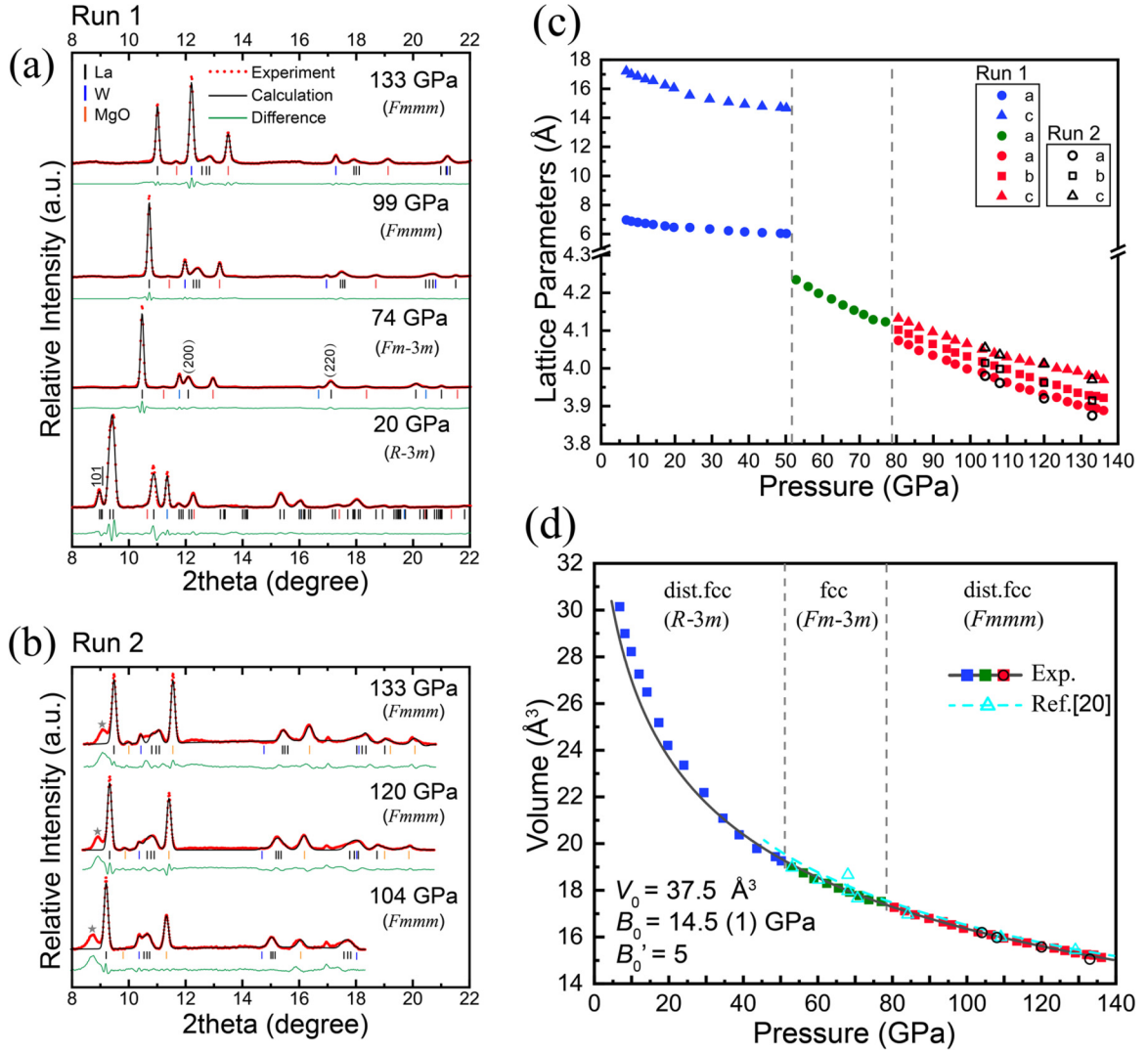


FIG. 1. (a), (b) Rietveld refinement of the experimental XRD pattern of La sample for two experimental runs. Positions of the Bragg reflections from La, MgO, and W gasket are marked with black, yellow, and blue vertical ticks, respectively. (c) The lattice parameters as a function of pressure. The straight dashed lines represent the phase boundaries. (d) Pressure-volume relations for La sample. The gray solid curve shows the third-order Birch-Murnaghan equation fitting to the experimental data (squares and circles). Triangles and cyan dashed curve represent the data from Ref. [20].

$4.3316 - 0.0033P$ (Å) and $b(P) = 4.3562 - 0.0032P$ (Å), while dc/dP is different: $c(P) = 4.3461 - 0.0028P$ (Å). In order to determine the parameters of the EOS, the obtained pressure-volume data were fitted by the third-order Birch-Murnaghan equation [33]:

$$P = \frac{3B_0}{2} \left[\left(\frac{V}{V_0} \right)^{-7/3} - \left(\frac{V}{V_0} \right)^{-5/3} \right] \times \left\{ 1 + \frac{3}{4}(B'_0 - 4) \left[\left(\frac{V}{V_0} \right)^{-2/3} - 1 \right] \right\}, \quad (1)$$

namely V_0 , B_0 , and B'_0 , where V_0 is the equilibrium cell volume, B_0 is the bulk modulus, and B'_0 is the derivative of bulk modulus with respect to pressure. The fitted parameters are $V_0 = 37.5$ (fixed) Å³, $B_0 = 14.5(1)$ GPa, and $B'_0 = 5$ (fixed), consistent with the result from Ref. [20], where H₂ and Ne

were used as the PTM. This also means that the nonhydrostatic pressure effect is not serious in this study. In Fig. 1(c), it is clearly seen that the lattice parameters changed discontinuously with pressures, indicating two phase transitions. In contrast, the volume data didn't show clear discontinuities up to the highest pressure, which is also observed in similar rare-earth metals [34–36]. This may be due to the fact that our observed distorted fcc phases *R $\bar{3}m$* and *Fm $\bar{3}m$* represent small different stacking sequences of fcc phase (*Fm $\bar{3}m$*) and thus may obscure observation of any volume discontinuity in the transitions.

To determine the boundary of phase transitions more accurately and investigate the pressure dependence of the superconducting transition of La, we conducted three runs of electrical measurements. The cell assembly used for the electrical resistance measurements is shown in Fig. 2. In order to take the nonhydrostatic effect into account and to reduce

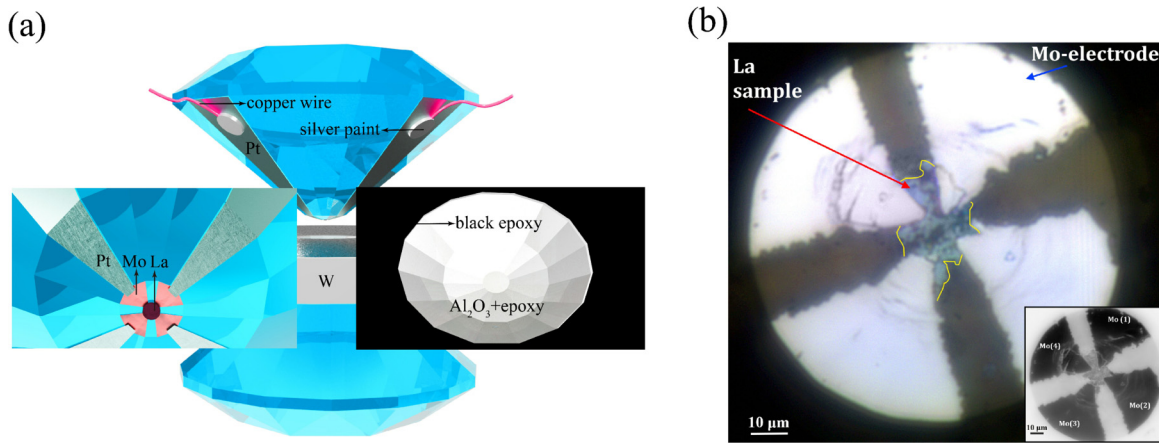


FIG. 2. (a) Schematic of the assembly used for the electrical resistance measurements. The sample chamber consisted of a tungsten outer gasket (W) with an insulating Al_2O_3 and epoxy. (b) Microphotograph of a sample at 140 GPa illuminated from the top. An inset shows the sample illuminated from the bottom.

the extension of the insulating layer under high pressures; we chose Al_2O_3 as the PTM and measured the resistance evolution of La as a function of temperature at various pressures in experimental runs 1–3, as shown in Figs. 3 and S4 [28]. The superconducting transition critical temperature T_c is defined near the temperature where the resistance begins to drop; the exact position depends on the details of the experiment. In Fig. 3, at ambient pressure, during the cooling from 300 to 1.5 K, the resistance first displays a typical metal-like behavior, then starts to drop to zero at 5.3 K. Further compression to 18 GPa makes the superconducting transition sharper, with the width around 0.5 K (from 10% to 90% of the normal-state resistance at T_{onset}), indicating a good homogeneity of

the superconducting phase. Below 50 GPa, pressure dependence of T_c shows the consistent tendency with the reported data [15,18] and two maxima at about 12 and 40 GPa were explained with the change of Fermi-surface topology. Upon further compression, the superconducting transition temperature decreased at different rates in two different intervals of pressure. There is an obvious turning point at about 78 GPa, which is associated with the start of distortion observed from the XRD data and it helps us to determine the phase boundary between $Fm\bar{3}m$ and $Fmmm$. In the range from 53 to 78 GPa where La should be in the fcc phase, the trend is relatively flat with a rate of -0.02 K/GPa. After the distortion occurred and lattice anisotropy increased with pressure, T_c decreased faster

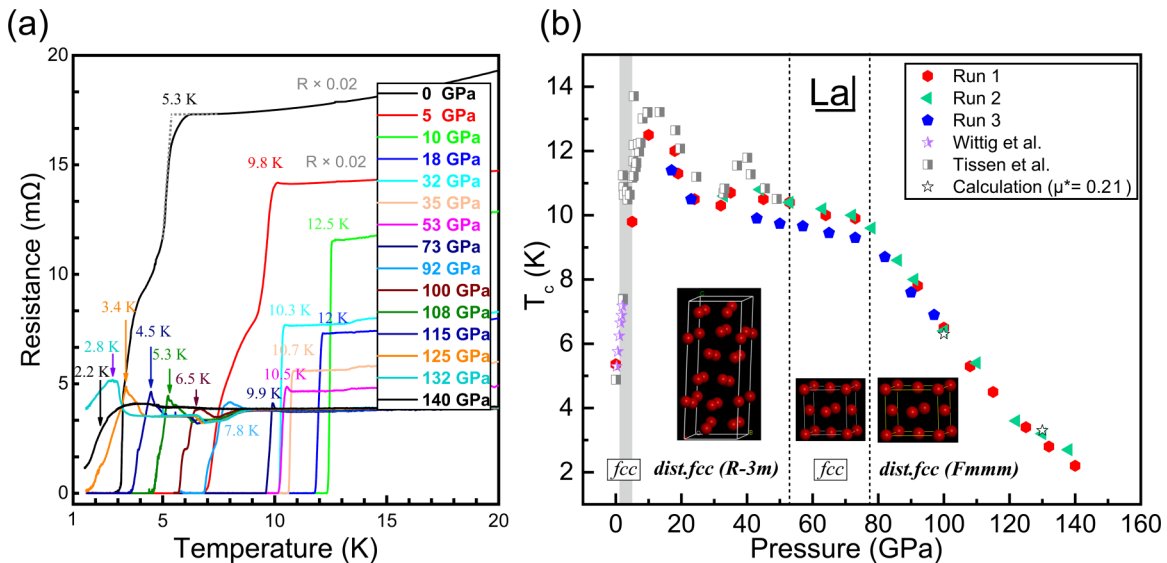


FIG. 3. (a) Resistance of the La sample as a function of temperature at various pressures during cooling in the experimental run 1. The gray characters represent the magnification of R . The lines with arrows show the definition of the superconducting transition temperature T_c . (b) The phase diagram and superconducting transition temperature T_c of La as a function of pressure. The red hexagon, green triangle, and blue pentagon symbols denote our experimental superconducting T_c data from runs 1–3. The purple asterisks and gray squares represent the data from Wittig *et al.* [15] and Tissen *et al.* [18]. The black dashed line marks the phase-transition boundaries determined by the present study.

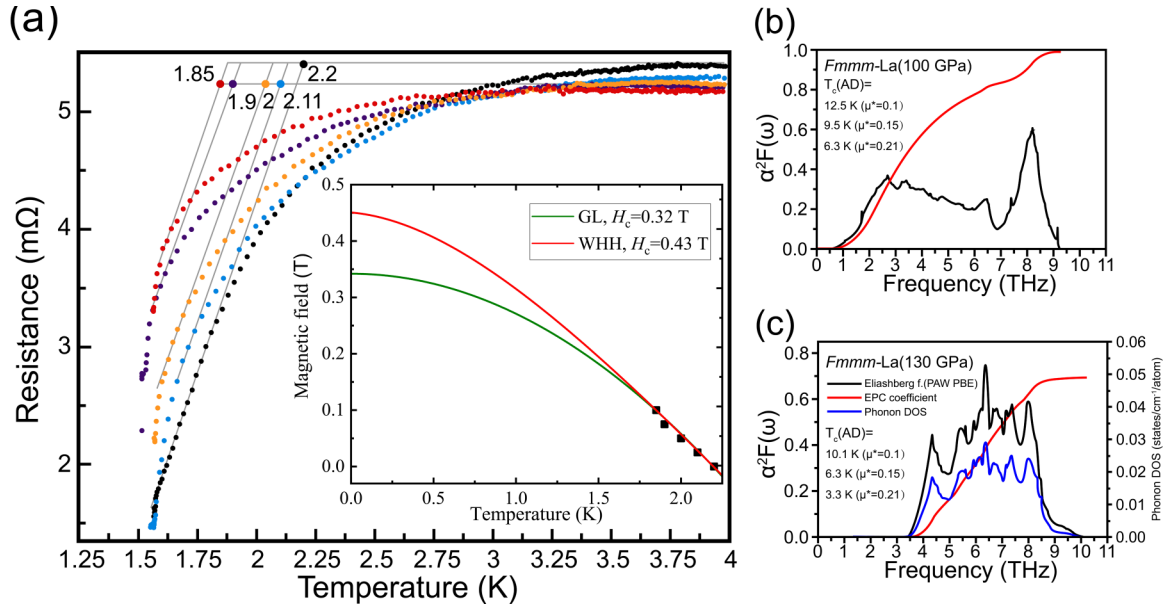


FIG. 4. (a) The experimentally measured superconducting transition of the La sample at 140 GPa with a magnetic field applied. In the inset, the dots show the measured values of T_c and magnetic field, while the solid lines represent fittings by the WHH and LG equations. (b), (c) The calculated superconducting parameters of the distorted fcc-La phase at 100 and 130 GPa.

at the rate of -0.13 K/GPa. We found the superconducting transitions can be triggered up to the maximum pressure of 140 GPa and fall down to 2.2 K. The beginning of the transition to a superconducting state at 140 GPa can also be fixed at the initial point of the resistance growth (~ 4.8 K), which is caused by the presence of distributed superconducting-normal grain boundaries [37]. Since the drop of resistance is not obvious in some runs of cooling and in order to get a further proof that the observed phenomenon is indeed superconducting transition, we measured the electrical resistance around the transition temperature in various external magnetic fields at 53 GPa (Fig. S5 [28]) and 140 GPa [Fig. 4(a)].

Figure 4(a) shows the measured resistance at 140 GPa with applied magnetic fields H of 0.025, 0.05, 0.075, and 0.1 T. The critical temperature T_c decreased with increasing magnetic field and much stronger fields are required to completely suppress superconductivity. To estimate the upper critical magnetic field $H_{c2}(0)$, we applied an extrapolation method combined with the Ginzburg-Landau (GL) equation [38]:

$$\mu_0 H_{c2}(T) = \mu_0 H_{c2}(0) \left(1 - \frac{T^2}{T_c^2}\right). \quad (2)$$

The extrapolation ($R^2 = 0.98$) of the transition temperature gives an estimate of $\mu_0 H_{c2}(0) = 0.32$ T. The Werthamer-Helfand-Hohenberg (WHH) model [39] for the critical magnetic field, simplified by Baumgartner [40],

$$\mu_0 H_{c2}(T) = \frac{\mu_0 H_{c2}(0)}{0.693} \left(\left(1 - \frac{T}{T_c}\right) - 0.153 \left(1 - \frac{T}{T_c}\right)^2 - 0.152 \left(1 - \frac{T}{T_c}\right)^4 \right) \quad (3)$$

leads to $\mu_0 H_{c2}(0) = 0.43$ T.

To obtain further insight, we have calculated the superconducting parameters of La at various pressures. To compare our calculations with the experimental results at 50 GPa, we first computed the superconducting parameters of the slightly distorted fcc-La ($R\bar{3}m$) using the Perdew-Zunger (PZ) and Perdew-Burke-Ernzerhof (PBE) pseudopotentials, obtaining $\lambda = 1.07$, $\omega_{\log} = 113$ K, and $T_c = 9.3$ K at $\mu^* = 0.1$ (50 GPa). The Eliashberg functions $\alpha^2 F(\omega)$ of the distorted fcc-La with different σ - broadenings (QE) at 50 GPa are presented in Fig. S6 [28]. The reported experimental T_c of 10.5 K at 50 GPa [18] is consistent with our experimental results (53 GPa, 10.5 K) and close to the calculated value (9.3 K). Thus, we are confident that our theoretical calculations of T_c and B_{c2} as a function of pressure are reliable. At 130 GPa, we took into account that the phonon spectrum of La ends at 350 cm^{-1} [~ 0.043 eV, Fig. 4(c)]. At such energies, the density of states near $E_F \pm \hbar\omega_{\max}$ is almost constant (≈ 10.05 states/Ry/La), which allows us to apply the “constant DOS approximation” [41] and take $\alpha^2 F(\omega)$ corresponding to an almost zero broadening in the QUANTUM ESPRESSO output. The results obtained with the Goedecker-Hartwigsen-Hutter-Teter PZ and Projector augmented-wave method (PAW) PBE pseudopotentials are the same: $\lambda = 0.69$, $\omega_{\log} = 288$ K, $T_c(AD) = 10.1$ K for $\mu^* = 0.1$ at 130 GPa. There is no significant differences in T_c and μ^* obtained with the different pseudopotentials. The experimental critical temperature of 2.8 K corresponds to an anomalous value of $\mu^* = 0.21$. At this Coulomb pseudopotential, the McMillan isotope coefficient $\beta = 0.21$ is quite small (it increases to 0.37 at $\mu^* = 0.15$), while the coherence length $\xi_{\text{BCS}} = 0.5\sqrt{\hbar/\pi e H_{c2}}$ is 23 nm, which is about 35% lower than for the metallic lanthanum at 0 GPa (36 nm) [42]. Calculations of T_c in *Fmmm*-La at 100 GPa [Fig. 4(b)] lead to the same Coulomb pseudopotential $\mu^* = 0.21$. The predicted slope of the $T_c(P)$ is close to the experimental data for the *Fmmm* phase from 78 to 140 GPa.

IV. CONCLUSIONS

In conclusion, we have studied the crystal structure and superconducting properties of the metallic La at pressures up to 140 GPa with nonhydrostatic PTM and discovered a distorted fcc-La phase (space group $Fmmm$). The superconducting transition has been detected in the distorted fcc-La at 9.6 K (78 GPa) and was found to decrease to 2.2 K (140 GPa) by means of the four-probe resistance measurements, and the experimentally obtained T_c for the $Fmmm$ phase exhibits an approximately linear decrease at a rate of -0.13 K/GPa, in the 78–140 GPa pressure range. We have investigated the influence of the external magnetic field (0–0.1 T) on T_c at 140 GPa which allowed us to estimate the upper critical magnetic field $\mu_0 H_{c2}(0)$ at 0.32–0.43 T, according to the GL and WHH models, respectively. The calculations of the electron-phonon interactions within the classical BCS mechanism point to an increased Coulomb pseudopotential $\mu^* = 0.21$, while the calculations using the usual μ^* interval (0.1–0.15) lead to an overestimated T_c (6.3–10.1 K at 130 GPa).

ACKNOWLEDGMENTS

This work was supported by the National Key R&D Program of China (Grant No. 2018YFA0305900), National Natural Science Foundation of China (Grants No. 51632002, No. 11974133, and No. 51720105007), National Key Research and Development Program of China (Grant No. 2016YFB0201204), Program for Changjiang Scholars and Innovative Research Team in University (Grant No. IRT_15R23), and National Fund for Fostering Talents of Basic Science (Grant No. J1103202). A.R.O. thanks Russian Ministry of Science and Higher Education (Grant 2711.2020.2 to leading scientific schools). The calculations were performed on the Rurik supercomputer at the MIPT and the Arkuda supercomputer of the Skolkovo Foundation. D.V.S. thanks the Russian Foundation for Basic Research (RFBR), grants No. 19-03-00100, 20-32-90099. I.A.T. and A.G.I. thanks Russian Science Foundation (Project No. 19-12-00414). Authors acknowledge beam scientists of the synchrotron beamline 16-BMD at Advanced Photon Source and the ID27 synchrotron beamline at the European Synchrotron Radiation Facility (Grenoble, France).

-
- [1] H. K. Onnes, *Commun. Phys. Lab. Univ. Leiden* **120b** (1911), reprinted in *Proc. K. Ned. Akad. Wet.* **13**, 1274 (1911).
- [2] A. Schilling, M. Cantoni, J. D. Guo, and H. R. Ott, *Nature (London)* **363**, 56 (1993).
- [3] G. Wu, Y. L. Xie, H. Chen, M. Zhong, R. H. Liu, B. C. Shi, Q. J. Li, X. F. Wang, T. Wu, Y. J. Yan, J. J. Ying, and X. H. Chen, *J. Phys.: Condens. Matter* **21**, 142203 (2009).
- [4] N. W. Ashcroft, *Phys. Rev. Lett.* **92**, 187002 (2004).
- [5] D. F. Duan, Y. X. Liu, F. B. Tian, D. Li, X. L. Huang, Z. L. Zhao, H. Y. Yu, B. B. Liu, W. J. Tian, and T. Cui, *Sci. Rep.* **4**, 6968 (2014).
- [6] I. Errea, M. Calandra, C. J. Pickard, J. Nelson, R. J. Needs, Y. W. Li, H. Y. Liu, Y. W. Zhang, Y. M. Ma, and F. Mauri, *Phys. Rev. Lett.* **114**, 157004 (2015).
- [7] A. P. Drozdov, M. I. Eremets, I. A. Troyan, V. Ksenofontov, and S. I. Shylin, *Nature (London)* **525**, 73 (2015).
- [8] M. Einaga, M. Sakata, T. Ishikawa, K. Shimizu, M. I. Eremets, A. P. Drozdov, I. A. Troyan, N. Hirao, and Y. Ohishi, *Nat. Phys.* **12**, 835 (2016).
- [9] X. L. Huang, X. Wang, D. F. Duan, B. Sundqvist, X. Li, Y. P. Huang, H. Y. Yu, F. F. Li, Q. Zhou, B. B. Liu, and T. Cui, *Nat. Sci. Rev.* **6**, 713 (2019).
- [10] M. Somayazulu, M. Ahart, A. K. Mishra, Z. M. Geballe, M. Baldini, Y. Meng, V. V. Struzhkin, and R. J. Hemley, *Phys. Rev. Lett.* **122**, 027001 (2019).
- [11] A. P. Drozdov, P. P. Kong, V. S. Minkov, S. P. Besedin, M. A. Kuzovnikov, S. Mozaffari, L. Balicas, F. F. Balakirev, D. E. Graf, V. B. Prakapenka, E. Greenberg, D. A. Knyazev, M. Tkacz, and M. I. Eremets, *Nature (London)* **569**, 528 (2019).
- [12] J. S. Schilling, in *Handbook of High Temperature Superconductivity: Theory and Experiment*, edited by J. R. Schrieffer and J. S. Brooks (Springer-Verlag, Hamburg, 2007), Chap. 11.
- [13] D. K. Finnemore, D. L. Johnson, J. E. Ostenson, F. H. Spedding, and B. J. Beaudry, *Phys. Rev.* **137**, A550 (1965).
- [14] T. Jarlborg, G. Anderson, B. Sundqvist, and Ö. Rapp, *J. Phys.: Condens. Matter* **1**, 8407 (1989).
- [15] J. Wittig, in *High Pressure in Science and Technology*, edited by C. Homan, R. K. MacCrone, and E. Whalley, MRS Symposia Proceedings No. 22 (North-Holland, Amsterdam, 1984), p. 17.
- [16] H. Balster and J. Wittig, *J. Low Temp. Phys.* **21**, 377 (1975).
- [17] F. Porsch and W. B. Holzapfel, *Phys. Rev. Lett.* **70**, 4087 (1993).
- [18] V. G. Tissen, E. G. Ponyatovskii, M. V. Nefedova, F. Porsch, and W. B. Holzapfel, *Phys. Rev. B* **53**, 8238 (1996).
- [19] J. S. Schilling, *Phys. C* **460**, 182 (2007).
- [20] Z. M. Geballe, H. Y. Liu, A. K. Mishra, M. Ahart, M. Somayazulu, Y. Meng, M. Baldini, and R. J. Hemley, *Angew. Chem. Int. Ed.* **57**, 688 (2018).
- [21] P. I. Dorogokupets and A. Dewaele, *High Pressure Res.* **27**, 431 (2007).
- [22] C. Prescher and V. B. Prakapenka, *High Pressure Res.* **35**, 223 (2015).
- [23] Y. Akahama and H. Kawamura, *J. Appl. Phys.* **100**, 043516 (2006).
- [24] P. Giannozzi, S. Baroni, N. Bonini, M. Calandra, R. Car, C. Cavazzoni, D. Ceresoli, G. Chiarotti, M. Cococcioni, I. Dabo, A. Dal Corso *et al.*, *J. Phys.: Condens. Matter* **21**, 395502 (2009).
- [25] S. Baroni, S. de Gironcoli, A. Dal Corso, and P. Giannozzi, *Rev. Mod. Phys.* **73**, 515 (2001).
- [26] S. Goedecker, M. Teter, and J. Hutter, *Phys. Rev. B* **54**, 1703 (1996).
- [27] P. B. Allen and R. C. Dynes, *Phys. Rev. B* **12**, 905 (1975).
- [28] See Supplemental Material at <http://link.aps.org/supplemental/10.1103/PhysRevB.102.134510> for equations for calculating T_c and related parameters; Structural information and results of X-ray diffraction studies; Superconducting properties.
- [29] K. Takemura, *J. Appl. Phys.* **89**, 662 (2001).

- [30] B. Li, C. Ji, W. G. Yang, J. Y. Wang, K. Yang, R. Q. Xu, W. J. Liu, Z. H. Cai, J. H. Chen, and H. K. Mao, *Proc. Natl. Acad. Sci. USA* **115**, 1713 (2018).
- [31] M. Seipel, F. Porsch, and W. B. Holzapfel, *High Pressure Res.* **15**, 321 (1997).
- [32] J. M. Leger, N. Yacoubi, and J. Loriers, *J. Solid State Chem.* **36**, 261 (1981).
- [33] F. Birch, *Phys. Rev.* **71**, 809 (1947).
- [34] G. N. Chesnut and Y. K. Vohra, *Phys. Rev. B* **62**, 2965 (2000).
- [35] M. Pravica, Z. Quine, and E. Romano, *Phys. Rev. B* **74**, 104107 (2006).
- [36] M. G. Pravica, E. Romano, and Z. Quine, *Phys. Rev. B* **72**, 214122 (2005).
- [37] C. J. Adkins, J. M. D. Thomas, and M. W. Young, *J. Phys. C: Solid State Phys.* **13**, 3427 (1980).
- [38] J. A. Woollam, R. B. Somoano, and P. O'Connor, *Phys. Rev. Lett.* **32**, 712 (1974).
- [39] N. R. Werthamer, E. Helfand, and P. C. Hohenberg, *Phys. Rev.* **147**, 295 (1966).
- [40] T. Baumgartner, M. Eisterer, H. W. Weber, R. Flükiger, C. Scheuerlein, and L. Bottura, *Supercond. Sci. Technol.* **27**, 015005 (2014).
- [41] W. Sano, T. Koretsune, T. Tadano, R. Akashi, and R. Arita, *Phys. Rev. B* **93**, 094525 (2016).
- [42] P. Loptien, L. Zhou, A. A. Khajetoorians, J. Wiebe, and R. Wiesendanger, *J. Phys.: Condens. Matter* **26**, 425703 (2014).